Electron Scattering Cross-Section Calculations for Atomic and Molecular Iodine

Harindranath B. Ambalampitiya [1,*], **Kathryn R. Hamilton** [2,*], **Oleg Zatsarinny** [2,†], **Klaus Bartschat** [2,*], **Matt A. P. Turner** [1], **Anna Dzarasova** [1] **and Jonathan Tennyson** [3,*]

[1] Quantemol Ltd., 320 City Rd, London EC1V 2NZ, UK; m_turner@quantemol.com (M.A.P.T.); adzarasova@quantemol.com (A.D.)
[2] Department of Physics and Astronomy, Drake University, Des Moines, IA 50311, USA
[3] Department of Physics and Astronomy, University College London, London WC1E 6BT, UK
[*] Correspondence: harin@quantemol.com (H.B.A.); kathryn.hamilton@drake.edu (K.R.H.); klaus.bartschat@drake.edu (K.B.); j.tennyson@ucl.ac.uk (J.T.)
[†] Deceased.

Abstract: Cross sections for electron scattering from atomic and molecular iodine are calculated based on the *R*-matrix (close-coupling) method. Elastic and electronic excitation cross sections are presented for both I and I_2. The dissociative electron attachment and vibrational excitation cross sections of the iodine molecule are obtained using the local complex potential approximation. Ionization cross sections are also computed for I_2 using the BEB model.

Keywords: electron-scattering; *B*-spline *R*-matrix; elastic; excitation; ionization; dissociative electron attachment; vibrational excitation

1. Introduction

Electron-scattering cross-section data for atomic and molecular iodine are important for plasma simulations and electric propulsion (EP) applications. In an EP system [1,2], an ionized gas (plasma) is accelerated electrostatically to generate thrust. This form of thrust generation significantly increases the payload-to-spacecraft mass ratio as compared to conventional chemical propulsion. To date, the state-of-the-art propellant gas for EP has been xenon (Xe) due to its high atomic mass, low ionization potential, and lack of toxicity. However, xenon has its own disadvantages. For example, it must be stored in high-pressure environments. Furthermore, Xe is not abundant in the Earth's crust, thus making it expensive and thereby limiting the industrial demand [3]. Therefore, replacements for Xe as a propellant have long been sought after. Iodine (I) is a viable candidate, as it not only has high atomic mass and low ionization potential, but can also be stored as a solid at lower pressures. Iodine is also more abundant in the Earth's crust (about 25,000 times compared to xenon [4]), thus making it a cheaper substitute.

The motivation for the present work is twofold. First, the recent developments in iodine-compatible EP thrusters such as iodine Hall-effect thrusters (iHETs) [5] resulted in a growing interest for $e^- - I/I_2$ scattering data for plasma simulations. In this type of thruster, electrons emitted from the cathode spiral around the thruster axis due to the combination of an axial electric and a radial magnetic field [2,6]. These electrons interact with the anode-fed gas, producing ions that are then accelerated by the electric field. Therefore, a systematic study of electron-driven processes and cross sections for $e^- - I/I_2$ collisions will help to improve the performance of iodine-based EP thrusters. As the second motivation, this work was initiated from one of the final projects that Oleg Zatsarinny was involved with before his untimely death on 2 March 2021. Therefore, the present paper is a dedication to his legacy remembering the pioneering work he did in the field of atomic, molecular, and optical (AMO) physics [7].

In the present paper, we employ the semirelativistic Breit-Pauli *B*-spline *R*-matrix (BPBSR) method to obtain cross section for $e^- - I$ collisions. For the molecular target, we perform electron scattering calculations using the UK molecular R-matrix codes [8,9] through using Quantemol expert systems [10,11]. Dissociative attachment and vibrational excitation cross sections are computed within the framework of the local complex potential (LCP) using a new code developed for this purpose.

Table 1 lists the summary of reactions that will be discussed in the present paper.

Table 1. Summary of the processes discussed in the present paper.

I	Reaction
Elastic scattering	$e^- + I(^2P_{3/2}) \rightarrow e^- + I(^2P_{3/2})$ $e^- + I(^2P_{1/2}) \rightarrow e^- + I(^2P_{1/2})$
Excitation	$e^- + I(^2P_{3/2}) \rightarrow e^- + I^*$ $e^- + I(^2P_{1/2}) \rightarrow e^- + I^*$
Ionization	$e^- + I(^2P_{3/2}) \rightarrow 2e^- + I^+$
I_2	Reaction
Elastic scattering	$e^- + I_2(X\,^1\Sigma_g^+) \rightarrow e^- + I_2(X\,^1\Sigma_g^+)$
Excitation	$e^- + I_2(X\,^1\Sigma_g^+) \rightarrow e^- + I_2^*$
Dissociative Electron attachment	$e^- + I_2(X\,^1\Sigma_g^+) \rightarrow I(^2P_{1/2}) + I^-(^1S)$
Vibrational excitation	$e^- + I_2(X\,^1\Sigma_g^+, \nu = 0) \rightarrow e^- + I_2(X\,^1\Sigma_g^+, \nu = \nu_f)$
Ionization	$e^- + I_2(X\,^1\Sigma_g^+) \rightarrow 2e^- + I_2^+$
Dissociative ionization	$e^- + I_2(X\,^1\Sigma_g^+) \rightarrow 2e^- + I + I^+$

2. Theoretical Method

In this section, we briefly describe the methodologies used for the atomic and molecular targets. We begin with the atomic target and then discuss the I_2 molecule.

2.1. Breit-Pauli B-spline R-matrix (BPBSR)

For the $e^- - I$ calculations, we used the semirelativistic Breit-Pauli *B*-spline *R*-matrix approach [12] with either 10 or 29 target states in the close-coupling expansion. These models will be referred to as BPBSR-10 and BPBSR-29 below. The target states were generated by running a collision calculation for $e^- - I^+$ and then looking for bound states. The BPBSR-10 model included the lowest 10 states (total) with configurations $5p^5$, $5p^46s$, and $5p^46p$, while the BPBSR-29 model included the next 19 states that could be built with the configurations $5p^45d$ and $5p^47s$, respectively.

Table 2 lists the excitation energies and configurations of the first ten excited states from ground-state iodine: $(4d^{10}5p^5)\,^2P_{3/2}$. The excitation energies are compared with the available data from NIST [13]. The overall agreement is not perfect, but sufficient for the accuracy needed for the purpose of the present paper. In fact, in order to make a direct comparison with state-selected experimental excitation results possible (should they become available), we adjusted the thresholds of these states to their NIST-recommended values.

2.2. Molecular R-matrix Method

The electron-scattering problem for a molecule involves two types of motion: the electron and the nuclear motion. The scattering electron plus the target molecule is conveniently solved using the fixed-nuclei approximation, i.e., the molecule remains frozen at equilibrium geometry. The electron collisions calculations are performed using the molecular *R*-matrix theory. For an extensive review of the *R*-matrix theory for molecular targets, the reader is referred to ref. [14].

Table 2. Configurations and excitation energies (eV) for the lowest ten states of I in the BPBSR calculations.

Configuration	BPBSR-29	NIST [13]
$4d^{10}5p^5$ $(^2P_{3/2})$	0.0000	0.0000
$4d^{10}5p^5$ $(^2P_{1/2})$	0.9529	0.9426
$4d^{10}5p^46s$ $(^4P_{5/2})$	7.2015	6.7736
$4d^{10}5p^46s$ $(^4P_{3/2})$	7.3939	6.9546
$4d^{10}5p^46s$ $(^2P_{3/2})$	7.9452	7.6646
$4d^{10}5p^46s$ $(^2P_{1/2})$	8.0447	7.8341
$4d^{10}5p^46p$ $(^4P_{5/2})$	8.1850	8.0473
$4d^{10}5p^46s$ $(^4P_{1/2})$	8.1898	7.5501
$4d^{10}5p^46p$ $(^4P_{3/2})$	8.2217	8.0577
$4d^{10}5p^46p$ $(^4D_{7/2})$	8.3228	8.1420

Electronic-structure calculations for I_2 were carried out using MOLPRO [15]. This involves the computation of the neutral as well as the resonance-state potential energy curves. For electronic excitation and elastic scattering calculations, we employ the *R*-matrix approach using the UKRMOL suite of codes [9] implemented in the Quantemol-N (QN) software [10]. The QN interface takes in the MOLPRO-optimized geometry of I_2 and the calculations are completed with the static-exchange plus polarization (SEP) scattering model [14]. A 6-311G GTO target basis set [16,17] is employed for all calculations and the *R*-matrix radius is set at 10 a_0. The same QN calculation setup is used to obtain the resonance parameters, which are required to treat the motion of the nuclei.

2.3. Local Complex Potential Approximation

The accurate treatment of the nuclear motion in the negative molecular-ion state is important for the calculations of resonant vibrational excitation and DEA cross sections. In the present work, we employ the LCP [18] approximation to treat the nuclear dynamics and use the resonant parameters obtained from fixed-nuclei *R*-matrix calculations as described in Section 2.2.

In the LCP approximation, the nuclear dynamics in the resonant state is governed by the Schrödinger equation

$$\frac{1}{2\mu}\frac{d^2}{dR^2}\chi(R) - \left[U^-(R) - i\frac{\Gamma(R)}{2} - E\right]\chi(R) = -V_{dk}(R)\zeta_\nu(R), \tag{1}$$

where μ is the reduced mass, $U^-(R)$ is the potential energy curve for the anion, $\Gamma(R)$ is the resonance width, $V_{dk} = \sqrt{\Gamma/2\pi}$ is the electron-capture amplitude into the resonance state, and $\zeta_\nu(R)$ is the vibrational wavefunction of the neutral molecule in its νth vibrational state. In brief, Equation (1) describes the dynamics of nuclei moving in a complex potential of which the real part is of either repulsive or attractive nature. The complex part of the energy is physically indicative of the decaying nature of the resonance state. It is important to note that in the case of broad shape resonances [18,19] or when the long-range dipolar interaction strongly affects the calculated cross sections, one has to go beyond the LCP approximation. However, employing the LCP approach in the present work is justified by the small resonance widths we obtained in our calculations (see below). We can construct a solution of Equation (1) in terms of the Green's function according to

$$\chi(R) = \int_0^\infty G(R, R')\lambda_\nu(R')dR', \tag{2}$$

where $\lambda_\nu(R) = -V_{dk}(R)\zeta_\nu(R)$ and the Green's function satisfies

$$\frac{1}{2\mu}\frac{d^2}{dR^2}G(R, R') - \left[U^-(R) - i\frac{\Gamma(R)}{2} - E\right]G(R, R') = \delta(R - R'). \tag{3}$$

Note that $G(R, R')$ has the same outgoing wave boundary condition as $\chi(R)$. The Green's function can be constructed from the solutions of the homogeneous equation by setting the RHS to zero in Equation (3). Next, let ψ^r and ψ^+ be the regular and irregular solutions of the homogeneous equation with the following asymptotic forms at $R \to \infty$:

$$\psi^r(R) \sim \psi^-(R) - \psi^+(R)S, \tag{4}$$

$$\psi^{\pm}(R) \sim \sqrt{\frac{\mu}{K}} \exp(\pm iKR). \tag{5}$$

Here S is the scattering matrix and $K^2 = 2\mu(E - U^-(R = \infty))$. With these two linearly independent solutions, we can construct the Green's function

$$iG(R, R') = \psi^r(R)\psi^+(R')\theta(R' - R) + \psi^r(R')\psi^+(R)\theta(R - R'), \tag{6}$$

where $\theta(R - R')$ is the Heaviside function. If the resonant state supports bound states, then the asymptotic conditions should be modified accordingly ($\chi(R \to 0, +\infty) \sim 0$). If the latter situation occurs, it is instructive to construct the Green's function directly by numerically solving the homogeneous equation. Then the Green's function reads

$$G(R, R') = \frac{1}{W}u(R_<)v(R_>), \; R_< = min(R, R'), R_> = max(R, R'), \tag{7}$$

where $u(R \to 0) \sim 0$, $v(R \to \infty) \sim 0$, and $W = v'u - u'v$. For the case of outgoing-wave boundary condition, substituting Equation (6) into Equation (2) yields

$$\chi(R) = -i\left[\psi^r(R) \int_R^\infty \psi^+(R')\lambda_\nu(R')dR' + \psi^+(R) \int_0^R \psi^r(R')\lambda_\nu(R')dR'\right]. \tag{8}$$

To obtain the regular solution ψ^r, one can start with the quasi-classical conditions (exponentially decaying solutions) in the classically-forbidden region and then integrate outward. For ψ^+, one can again start with the boundary conditions in Equation (5) and then integrate inward. Normalization procedures of the numerical solutions can be avoided if Equation (7) for the Green's function is used directly.

The DEA cross section σ_{DEA}^ν is given by [20]

$$\sigma_{DEA}^\nu = g\,\frac{\pi^2}{k_\nu^2}\frac{K}{\mu} \lim_{R \to \infty} |\chi(R)|^2, \tag{9}$$

where $k_\nu^2/2$ is the energy of the incident electron and K is defined before in Equation (5). The symbol g denotes the ratio of the statistical weights of the resonant state and the target electronic state. The asymptotic factor in Equation (9) can be obtained from the second term in Equation (8) according to

$$\lim_{R \to \infty} |\chi(R)|^2 = \frac{\mu}{K}\left|\int_0^\infty \psi^r(R')\lambda_\nu(R')dR'\right|^2. \tag{10}$$

The vibrational excitation cross section is given by [21] as

$$\sigma_{\nu \to \nu'} = \frac{2\pi^3}{k^2}g\left|< \zeta_{\nu'}|V_{dk'}|\chi >\right|^2. \tag{11}$$

For the evaluation of the matrix elements, we must now use the full solution for χ given in Equation (8). It is well known that the local theory fails to describe the magnitude of the cross section near threshold. The local theory yields an infinite cross section for $E \to 0$. However, according to the Wigner threshold law [22], the exothermic DEA cross section for nonpolar molecules at threshold should depend on energy E as $E^{l-1/2}$ [23], where l is the lowest orbital angular momentum allowed by the symmetry of the resonant state. To modify this deficiency in the local theory, we introduce a correction factor $C(R)$ [21] into the capture amplitude: $V_{dk} = C(R)\sqrt{\Gamma/2\pi}$. The correction factor $C(R)$ has the form [21]

$$C(R) = \left(\frac{k^2}{2E_r(R)}\right)^{\tau/2}, \ k^2 < 2E_r, \tag{12}$$

where the resonance energy $E_r(R) = U^-(R) - U^0(R)$, and $U^0(R)$ is the potential energy of the neutral molecule. For $k^2 \geq 2E_r$ or sufficiently far away from the threshold, our calculations showed that $C(R)$ does not play a significant role and can be taken as unity. For nonpolar molecules, the threshold exponent is $\tau = l + 1/2$ according to the Wigner law.
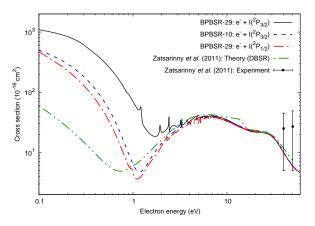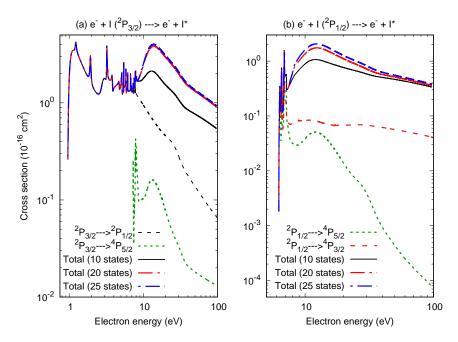
3. Results

3.1. Atomic Iodine

Figure 1 shows the elastic scattering cross sections for atomic iodine when it is in the ground and the first excited state (BSR-29 only). The elastic cross section exhibits a Ramsauer minimum, which is clearly visible for the $4d^{10}5p^5$ ($^2P_{1/2}$) state at about 1 eV. Previous fullrelativistic D(irac) *B*-Spline *R*-matrix (DBSR) [24] calculations by Zatsarinny et al. reported a Ramsauer minimum at lower energy of 0.7 eV [25]. Their cross section for energies less than about 0.1 eV is about one order of magnitude smaller than the present results. This is an indication of the extreme sensitivity of the predictions in this energy regime. In contrast to the present calculation, the DBSR model contained configurations that were built with pseudo-orbitals to specifically account for polarization effects on the two lowest states. The difference by an order of magnitude at 0.1 eV drops to a factor of $\approx$2 around 0.5 eV, and the results are much closer beyond the Ramsauer minimum.

The two experimental data points at 40 and 50 eV are taken from ref. [25] (while the uncertainties are larger than the differences between the values at the two energies, it appears as if the two points were accidentally interchanged between Table II (correct) and Figure 3 of [25]). No experimental data below 40 eV were found in the literature. Without experimental data, it is difficult to judge which of these theoretical predictions is most reliable. If accurate results at these very low energies were required, a separate study should be performed that is specifically devoted to this energy regime.

Figure 2 exhibits electronic excitation cross sections from the $4d^{10}5p^5$ ($^2P_{3/2}$) and $4d^{10}5p^5$ ($^2P_{1/2}$) states. In each case, cross sections for excitation into the next two higher levels are plotted. For the $^2P_{3/2}$ state, specifically, the next higher level is the $^2P_{1/2}$ state with the same configuration but a different total electronic angular momentum, resulting in a fine-structure splitting of nearly one eV (cf. Table 2). The total cross section is obtained by summing the partial excitation cross sections to 10, 20, and 25 final states, respectively. As seen from Figure 2, the total excitation cross section converges after including about 20 target states. Unfortunately, no experimental data for electron-impact excitation of atomic iodine were found in the literature.

Figure 1. Elastic scattering cross section as a function of the electron energy. Cross sections for the ground state obtained in the BPBSR-10 and BPBSR-29 models are shown, as well the BPBSR-29 prediction for the first excited state and the result from the DBSR calculation reported by Zatsarinny et al. [25]. The experimental data at 40 eV and 50 eV are taken from ref. [25].

Figure 2. Electron-impact excitation cross section from (**a**) the ground state and (**b**) the first excited state of atomic iodine. The total cross sections shown are obtained by summing the partial cross sections into 10, 20, and 25 final states as shown in the legend.
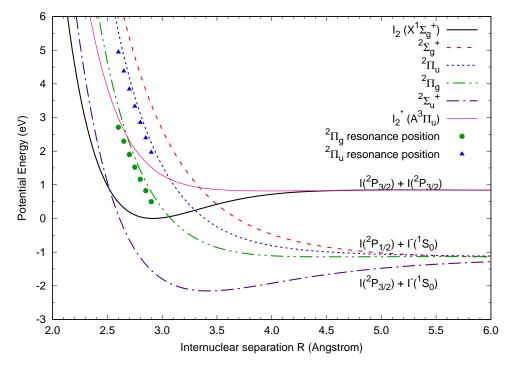
3.2. Molecular Iodine

Table 3 lists the ground-state properties of I_2. The results were obtained by performing MOLPRO-CASSCF calculations with the 6-311G basis set. The ground-state configuration of I_2 is $(1\text{-}13A_g, 1\text{-}6B_{3u}, 1\text{-}6B_{2u}, 1\text{-}2B_{1g}, 1\text{-}12B_{1u}, 1\text{-}6B_{2g}, 1\text{-}6B_{3g}, 1\text{-}2A_u)^2$.

Table 3. Ground-state properties of I_2.

Property	Present Value	Value in [26]
Ground state energy (Hartree)	$-13{,}833.5045$	$-13{,}834.05986$
Bond length (Å)	2.8102	2.6655
Vibrational frequency (cm^{-1})	207.71	214.502
Symmetry	D_{2h}	D_{2h}

For the calculations of the cross sections, accurate details of the neutral and anion potential energy surfaces (PES) are important. In the present work, we obtained the PESs using MOLPRO (CASSCF with the 6-311G basis). In Figure 3, the ab initio calculations for the potential-energy curves of the neutral, anion, and the lowest excited state of I_2 are shown. For the anion state, several scattering-state symmetries are considered. The calculated resonance positions for the $^2\Pi_g$ and $^2\Pi_u$ states using the *R*-matrix approach agree well with the standard MOLPRO bound-state calculations. This confirms the accuracy of the crossing points of the neutral and anion potential curves.

For calculating the resonance parameters, we first obtain the eigenphase sum for the relevant scattering symmetry at several internuclear separations. The scattering calculations are performed with the SEP scattering model. In QN, the eigenphase sum is fitted to a Breit-Wigner form and produces the corresponding resonance widths and positions [27]. Figure 4 shows the eigenphase sum for $^2\Pi_g$ symmetry evaluated at several internuclear separations near the equilibrium geometry. This illustrates the stability in our scattering calculations for the resonance parameters. In Figure 4, the calculated resonance widths for the $^2\Pi_g$ and $^2\Pi_u$ resonances are shown as function of the internuclear separation.

Figure 3. Ab initio calculations of the neutral and anion (resonance) potential energy curves. MOLPRO results are shown for the four resonant symmetries $^2\Sigma_g^+$, $^2\Pi_u$, $^2\Sigma_u^+$, and $^2\Pi_g$. The $^2\Pi_g$ and $^2\Pi_u$ resonance positions calculated with the *R*-matrix method agree well with the bound-state results.

Figure 4. (**a**) Eigenphase sum for the $^2\Pi_g$ symmetry evaluated at several internuclear separations *R*. (**b**) Resonance widths $\Gamma(R)$ for the two scattering symmetries considered in the present calculations.
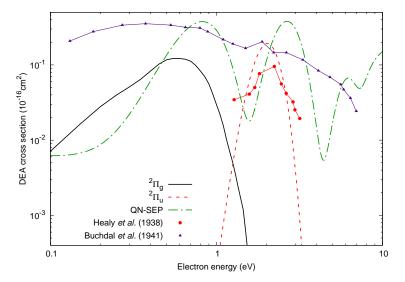
3.2.1. Dissociative Electron Attachment

Figure 5 shows the DEA cross section of I_2 in the energy range 0.1–10.0 eV. The cross sections are obtained for two scattering symmetries in the LCP approximation. The present local calculations show peaks around 0.6 and 2.0 eV, which agree with the low-energy peaks reported in ref. [28]. The experimental data from ref. [29] exhibit a smaller peak
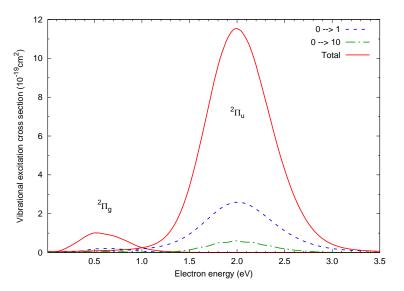
similar to the $^2\Pi_u$ resonance. We also show the DEA cross section estimates [30] obtained from QN. As seen in Figure 5, SEP results show good agreement with the LCP calculations. However, the peaks are shifted to higher energies by about 0.5 eV. For the QN results we set the vibrational frequency at 214 cm^{-1}, dissociation energy at 1.58 eV, and electron affinity at 3.059 eV [13].

3.2.2. Vibrational Excitation

The VE cross sections from the ground vibrational state to the $\nu = 1$ and $\nu = 10$ states are shown in Figure 6. As the resonant states ($^2\Pi_u, {}^2\Pi_g$) considered in the present work are purely repulsive, only isolated peaks in the cross section around 0.5 and 2 eV are observed. The total vibrational excitation cross section is obtained by summing the cross sections into the $\nu = 0, 1, \ldots, 10$ channels.

Figure 5. DEA cross section of I$_2$. In the LCP framework (solid and dashed lines), the cross section shows maxima at 0.6 and 2 eV similar to Buchdal et al. [28]. The results from Healy et al. [29] agree with the $^2\Pi_u$ resonance position. QN's SEP calculations (dashed-dotted line) exhibit the same structures with shifted peaks compared to the present results.
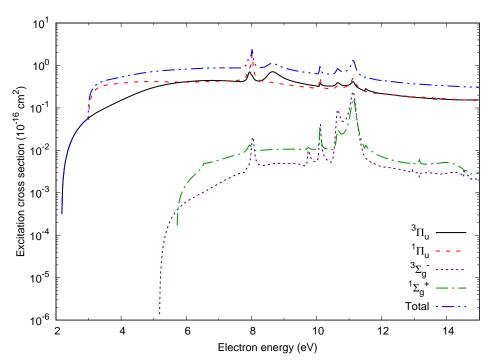

Figure 6. VE cross sections obtained for the $^2\Pi_g$ and $^2\Pi_u$ symmetries. Dashed and dashed-dotted lines show the $\nu = 0 \rightarrow 1, 10$ results and the solid line shows total VE cross section, respectively.

3.2.3. Electron-Impact Excitation

The excitation cross sections are computed with the ground-state configuration mentioned at the beginning of Section 3. In configuration-interactions (CI) calculations, only four electrons are allowed in the active space consisting of 14–16a_g, 13b_{1u}, 6b_{2g}, 6b_{3g} orbitals. Figure 7 exhibits the cross sections for electronic excitation into the lowest four excited states with term symbols $^3\Pi_u$, $^1\Pi_u$, $^3\Sigma_g^-$, and $^1\Sigma_g^+$, respectively. Table 4 lists the vertical excitation energies of the excited states from the ground state. Reference data from the theoretical work of Mulliken [31] are also given.

Table 4. Vertical excitation energies (eV) from the ground state.

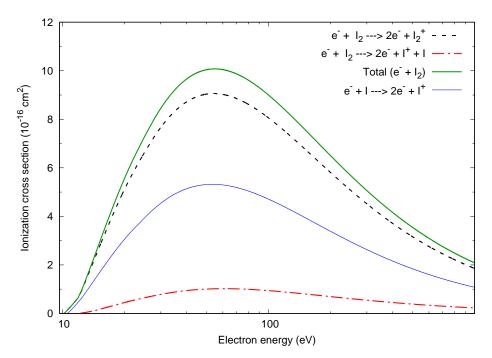| State	Energy	Ref. [31]
$^3\Pi_u$	2.18	2.37
$^1\Pi_u$	3.00	2.38
$^3\Sigma_g^-$	5.18	3.9
$^1\Sigma_g^+$	5.7	–

Figure 7. Cross sections for excitation to the $^3\Pi_u$, $^1\Pi_u$, $^3\Sigma_g^-$, and $^1\Sigma_g^+$ states from the ground state.

3.2.4. Ionization

Figure 8 shows the electron-impact ionization cross sections of I and I_2 obtained using the binary-encounter Bethe (BEB) method [32]. These calculations were set up in QEC [11] after implementing the use of effective-core potentials (ECP) [33]. For the estimate of partial ionization cross sections, we used approximate branching ratios of 0.1 and 0.9 for reactions leading to I_2^+, and I^+/I products, respectively. The ECP calculations give the ionization threshold for I_2 as 10.19 eV. For dissociative ionization, the threshold was taken as 11.94 eV [13].

3.2.5. Elastic Scattering

In this section, we present the results for elastic scattering of electron from the I_2 molecule. Figure 9 shows the total elastic scattering and momentum transfer cross sections. A strong spike in the elastic cross section is observed for electron energies at 1 eV, which corresponds to the Π_g resonance.

Figure 8. Electron-impact ionization cross section obtained for I and I_2. Also shown are the partial ionization cross sections for I_2 leading to products I_2^+ (dashed line) and I^+ (dashed-dotted line).
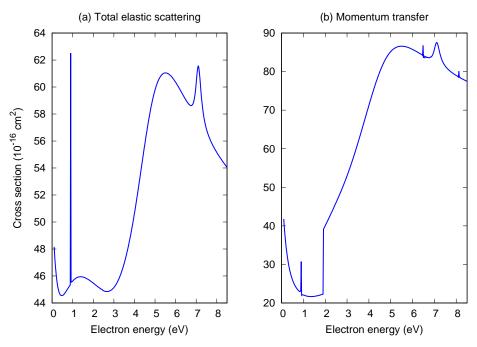

Figure 9. (**a**) Total elastic scattering and (**b**) momentum transfer cross section.

4. Conclusions and Outlook

In the present work, we computed cross sections for electron collisions with atomic and molecular iodine. For the atomic case, we employed a semirelativistic *B*-spline *R*-matrix approach and compared the results obtained with 10 and 29 states included in the close-coupling expansion. For elastic scattering, we also compared with predictions from an earlier fullrelativistic DBSR calculation [25].

The overall agreement between predictions from these models is good for energies above the Ramsauer minimum at ≈1 eV, while very large differences were found at lower energies. This suggests that a semirelativistic approach to the collision problem is generally sufficient, but also that much more work would be required before one can be confident

in any of these predictions at thermal energies. Unfortunately, no experimental data at all are available for comparison in the low-energy regime, and the uncertainties of the two published experimental points at 40 eV and 50 eV were estimated to be about 80% of their actual values. Nevertheless, we believe that the present calculations represent a valuable basis for further studies, and that they should significantly improve the available database to describe energy-loss processes in collisions between electrons and atomic iodine.

We also carried out *R*-matrix calculations to obtain excitation and elastic scattering cross sections for molecular iodine. Electronic-excitation and elastic electron-scattering cross sections for I_2 were obtained using the Quantemol-N expert system. Compared to previous work reported in [34], we used an enhanced basis set (6-311G vs. 3-211G), which led to more accurate resonance parameters. In addition, we computed resonant vibrational excitation and dissociative attachment to I_2 in the framework of the LCP approximation. Improving on these calculations will require the use ECPs in the scattering calculations; this is currently being investigated.

Diatomic halogens are highly reactive gases that can bleach the surfaces of the electron spectrometer causing changes in the contact potentials. This makes experiments for low-energy DEA and VE to be extremely difficult. After comparing the present DEA calculations with the only available experimental data, low-energy peaks in the experimental cross section were assigned to the $^2\Pi_g$ and $^2\Pi_u$ resonances of I_2. Similar observations were made by Tam and Wong [35] who reported three resonance peaks for 0–8 eV electrons. Typically, DEA to diatomic halogens is exothermic and results in large cross sections at low energy. In the case of F_2 and Cl_2, the low-energy DEA cross section is dominated by the Σ_u^+ symmetry [36–38]. For I_2, however, the potential-energy curve for Σ_u^+ state crosses the neutral curve further left to the Franck-Condon region. This suggests that the contribution from the Σ_u^+ state should be rather weak. Similar observations in DEA to Br_2 were reported by Kurepa et al. [39]. More experimental evidence and calculations beyond the LCP approximation are necessary to characterize the low-energy behavior of DEA to I_2. The results from the DEA estimator [30] in QN showed overall agreement with the LCP results in the considered energy range. This suggests the applicability of the DEA estimator program for complicated molecules where the local calculations become computationally challenging.

Abbreviations

The following abbreviations are used in this manuscript:

BEB	Binar Encounter Bethe
BPBSR	Breit-Pauli *B*-Spline *R*-matrix
CASSCF	Complete Active Space Self-Consistent Field
DEA	Dissociative Electron Attachment
ECP	Effective core potential
EP	Electric Propulsion
LCP	Local Complex Potential
QEC	Quantemol Electron Collisions
QN	Quantemol-N
VE	Vibrational Excitation

References

1. Choueiri, E. *Plasma Propulsion-McGraw-Hill Encyclopedia of Science and Technology*; McGraw-Hill: New York, NY, USA, 2007.
2. Goebel, D.M.; Katz, I. *Fundamentals of Electric Propulsion: Ion and Hall Thrusters*; JPL: Pasadena, CA, USA, 2008.
3. Kieckhafer, A.; King, L.B. Energetics of Propellant Options for High-Power Hall Thrusters. *J. Propuls. Power* **2007**, *23*, 21.
4. Dressler, R.A.; Chiu, Y.H.; Levandier, D. Propellant alternatives for ion and Hall effect thrusters. In Proceedings of the 38th Aerospace Sciences Meeting and Exhibit, Reno, NV, USA, 10–13 January 2000.
5. Smith, T.D.; Kamhawi, H.; Hickman, T.; Haag, T.; Dankanich, J.; Polzin, K.; Byrne, L.; Szabo, J. *Overview of NASA Iodine Hall Thruster Propulsion System Development*; Technical Report; NASA: Washington, DC, USA, 2016.
6. Kaganovich, I.D.; Smolyakov, A.; Raitses, Y.; Ahedo, E.; Mikellides, I.G.; Jorns, B.; Taccogna, F.; Gueroult, R.; Tsikata, S.; Bourdon, A.; et al. Physics of $E \times B$ discharges relevant to plasma propulsion and similar technologies. *Phys. Plasmas* **2020**, *27*, 120601.
7. Bartschat, K.; Fischer, C.F.; Grum-Grzhimailo, A.N. A Tribute to Oleg Zatsarinny (1953–2021): His Life in Science. *Atoms* **2021**, *9*, 53.
8. Carr, J.M.; Galiatsatos, P.G.; Gorfinkiel, J.D.; Harvey, A.G.; Lysaght, M.A.; Madden, D.; Mašín, Z.; Plummer, M.; Tennyson, J.; Varambhia, H.N. UKRmol: A low-energy electron- and positron-molecule scattering suite. *Eur. Phys. J. D* **2012**, *66*, 58.
9. Mašín, Z.; Benda, J.; Gorfinkiel, J.D.; Harvey, A.G.; Tennyson, J. UKRmol+: A suite for modelling electronic processes in molecules interacting with electrons, positrons and photons using the R-matrix method. *Comp. Sci. Commun.* **2019**, *249*, 107092.
10. Tennyson, J.; Brown, D.B.; Munroy, J.J.; Rozum, I.; Varambhia, H.N.; Vinci, N. Quantemol-N: An expert system for performing electron molecule collision calculations using the R-matrix method. *J. Phys. Conf. Ser.* **2007**, *86*, 012001.
11. Cooper, B.; Tudorovskaya, M.; Mohr, S.; O'Hare, A.; Hanicinec, M.; Dzarasova, A.; Gorfinkiel, J.D.; Benda, J.; Mašín, Z.; Al-Refaie, A.F.; et al. Quantemol Electron Collisions (QEC): An Enhanced Expert System for Performing Electron Molecule Collision Calculations Using the R-Matrix Method. *Atoms* **2019**, *7*, 97.
12. Zatsarinny, O. BSR: B-spline atomic R-matrix codes. *Comp. Phys. Commun.* **2006**, *174*, 273.
13. NIST Chemistry WebBook. Available online: https://webbook.nist.gov/chemistry/ (accessed on 21 September 2021).
14. Tennyson, J. Electron–molecule collision calculations using the *R*-matrix method. *Phys. Rep.* **2010**, *491*, 29.
15. Werner, H.J.; Knowles, P.J.; Knizia, G.; Manby, F.R.; Schütz, M. Molpro: A general-purpose quantum chemistry program package. *Rev. Comp. Mol. Sci.* **2011**, *2*, 242.
16. Schuchardt, K.L.; Didier, B.T.; Elsethagen, T.; Sun, L.; Gurumoorthi, V.; Chase, J.; Li, J.; Windus, T.L. Basis Set Exchange: A Community Database for Computational Sciences. *J. Chem. Inf. Model.* **2007**, *47*, 1045.
17. Glukhovtsev, M.N.; Pross, A.; McGrath, M.P.; Radom, L. Extension of Gaussian-2 (G2) theory to bromine- and iodine-containing molecules: Use of effective core potentials. *J. Chem. Phys.* **1995**, *103*, 1878.
18. Bardsley, J.N.; Mandle, F. Resonant scattering of electrons by molecules. *Rep. Prog. Phys.* **1968**, *31*, 471.
19. Domcke, W. Theory of resonance and threshold effects in electron-molecule collisions: The projection-operator approach. *Phys. Rep.* **1991**, *208*, 97.
20. Bardsley, J.N. Configuration interaction in the continuum states of molecules. *J. Phys. B At. Mol. Phys.* **1968**, *1*, 349.
21. Bardsley, J.N. Molecular resonance phenomena. In *Electron-Molecule and Photon-Molecule Collisions*; Rescigno, T., McKoy, V., Schneider, B., Eds.; Plenum: New York, NY, USA, 1979.
22. Wigner, E.P. On the Behavior of Cross Sections Near Thresholds. *Phys. Rev.* **1948**, *73*, 1002.
23. Fabrikant, I.I.; Hotop, H. Low-energy behavior of exothermic dissociative electron attachment. *Phys. Rev. A* **2001**, *63*, 022706.
24. Zatsarinny, O.; Bartschat, K. Relativistic *B*-spline *R*-matrix method for electron collisions with atoms and ions: Application to low-energy electron scattering from Cs. *Phys. Rev. A* **2008**, *77*, 062701.
25. Zatsarinny, O.; Bartschat, K.; Garcia, G.; Blanco, F.; Hargreaves, L.R.; Jones, D.B.; Murrie, R.; Brunton, J.R.; Brunger, M.J.; Hoshino, M.; et al. Electron-collision cross sections for iodine. *Phys. Rev. A* **2011**, *83*, 042702.

26. Computational Chemistry Comparison and Benchmark Database. Available online: https://cccbdb.nist.gov/ (accessed on 21 September 2021).
27. Tennyson, J.; Noble, C.J. RESON—A program for the detection and fitting of Breit-Wigner resonances. *Comp. Phys. Commun.* **1984**, *33*, 421.
28. Buchdal, R.J. Negative Ion Formation in Iodine Vapor by Electron Impacts. *J. Chem. Phys.* **1941**, *9*, 146.
29. Healy, R.H. The behaviour of electrons in iodine vapour. *Philos. Mag. J. Sci.* **1938**, *26*, 940.
30. Munro, J.J.; Harrison, S.; Fujimoto, M.M.; Tennyson, J. A dissociative electron attachment cross-section estimator. *Phys. Conf. Ser.* **2012**, *388*, 012013.
31. Mulliken, R.S. Iodine Revisited. *J. Chem. Phys.* **1971**, *55*, 288.
32. Kim, Y.K.; Rudd, M.E. Binary-encounter-dipole model for electron-impact ionization. *Phys. Rev. A* **1994**, *50*, 3954.
33. Graves, V.; Cooper, B.; Tennyson, J. The efficient calculation of electron impact ionization cross sections with effective core potentials. *J. Chem. Phys.* **2021**, *154*, 114104.
34. Yadav, H.; Vinodhkumar, M.; Limbachiya, C.; Vinodhkumar, P.C.; Mason, N.J. Low energy electron interactions with Iodine molecule (I_2). *J. Quant. Spectrosc. Radiat. Transf.* **2020**, *250*, 107035.
35. Tam, W.C.; Wong, S.F. Dissociative attachment of halogen molecules by 0–8 eV electrons. *J. Chem. Phys.* **1978**, *68*, 5626.
36. Fabrikant, I.I.; Eden, S.; Mason, N.J.; Fedor, J. Recent Progress in Dissociative Electron Attachment: From Diatomics to Biomolecules. *Adv. At. Mol. Opt. Phys.* **2017**, *66*, 545.
37. Ruf, M.W.; Barsotti, S.; Braun, M.; Hotop, H.; Fabrikant, I.I. Dissociative attachment and vibrational excitation in low-energy electron collisions with chlorine molecules. *J. Phys. B At. Mol. Opt. Phys.* **2003**, *37*, 41.
38. Braun, M.; Ruf, M.W.; Fabrikant, I.I.; Hotop, H. Observation of *p*-Wave Threshold Behavior in Electron Attachment to F_2 Molecules. *Phys. Rev. Lett.* **2007**, *99*, 253202.
39. Kurepa, M.V.; Babic, D.S.; Belic, D.S. Electron-bromine-molecule total ionisation and electron attachment cross sections. *J. Phys. B. At. Mol. Phys.* **1981**, *14*, 375.